Weierstraß-Institut
für Angewandte Analysis und Stochastik

im Forschungsverbund Berlin e.V.

Preprint ISSN 0946 – 8633

Traveling wave modeling of dynamics in semiconductor ring lasers

Mindaugas Radziunas[1]

submitted: 28 March 2008

[1] Weierstraß-Institut
für Angewandte Analysis und Stochastik
Mohrenstrasse 39
D – 10117 Berlin
Germany
E-Mail: radziunas@wias-berlin.de

No. 1315
Berlin 2008

2000 *Mathematics Subject Classification.* 78-04,78A60,35-04,78-05,35Q60,35B35.

Key words and phrases. semiconductor ring laser, traveling wave model, switching, alternate oscillations, bistability, unidirectional, optical modes, analysis .

2008 Physics and Astronomy Classification Scheme. 42.55.Px 42.60.-v 02.30.Jr 02.60.Cb.
Supported by the DFG Research Center MATHEON "Mathematics for key technologies".

Edited by
Weierstraß-Institut für Angewandte Analysis und Stochastik (WIAS)
Mohrenstraße 39
10117 Berlin
Germany

Fax: + 49 30 2044975
E-Mail: preprint@wias-berlin.de
World Wide Web: http://www.wias-berlin.de/

Abstract

We use the traveling wave model for simulating and analyzing nonlinear dynamics of complex semiconductor ring laser devices. This modeling allows to consider temporal-spatial distributions of the counter-propagating slowly varying optical fields and the carriers, what can be important when studying non-homogeneous ring cavities, propagation of short pulses or fast switching. By performing numerical integration of the model equations we observe several dynamic regimes as well as transitions between them. The computation of ring cavity modes explains some peculiarities of these regimes.

1 INTRODUCTION

Semiconductor ring lasers (SRLs) are interesting devices for their applications in photonic integrated circuits [1, 2, 3]. To simulate the SRL a two-mode ODE model consisting of a pair of complex equations for the counter-propagating longitudinal modes and a rate equation for the carrier density is frequently used [4, 5]. It can give an adequate explanation of different operation regimes such as alternating oscillations, bidirectional and unidirectional continuous wave (cw) states or transitions between these regimes. This rather simple model admits a variety of ODE analysis methods. For example, it can be studied by means of numerical path-following and bifurcation analysis tools [6], or by means of asymptotic analysis methods [7].

However, this model can not recover different multi-mode effects of SRLs such as modelocking [8] or transitions between multiple longitudinal modes [9]. Moreover, it is based on mean-field approximations and does not allow considering inhomogeneity of laser parameters and dynamical variables along the ring cavity. That is, its usage for modeling of long SRLs with non-homogeneous parameters or for description of propagating short pulses along the cavity remains questionable.

There exist different approaches allowing to overcome the limitations listed above. The representation of the optical field as a superposition of several coupled longitudinal modes yields an ODE model [10] describing multi-mode dynamics, but not longitudinal inhomogeneities of SRLs. Another approach allowing to take into account both above mentioned effects can be given by a DDE model [11], which was successfully used for studying modelocking (ML) regimes in semiconductor lasers. This model, however, assumes a unidirectional ring configuration.

In the present paper we discuss a PDE modeling approach with a single spatial dimension corresponding to the longitudinal direction along the ring cavity. This

model considers the clockwise (CW) and counter-clockwise (CCW) propagating slowly varying optical fields governed by the traveling wave (TW) equations [12], which are mutually coupled through linear backscattering terms, through nonlinear cross- and self- saturations, and are both coupled to the spatially parameterized carrier rate equation. This approach allows simulating ring structures consisting from differently driven sections, considering longitudinal distributions of the carriers and of the optical fields, which can be also expressed as a superposition of the longitudinal optical modes. Moreover, this modeling can take into account optical injections, localized reflections and, therefore, delayed feedbacks of the optical fields.

Comparing to the above listed models, our TW modeling approach is computationally more demanding and is much more difficult to analyze. Fortunately, for these reasons we could adapt our own software package `LDSL-tool` [13], originally developed to simulate and to analyze [14, 15] different linear multisection semiconductor lasers.

The main aim of our paper is to introduce the basic structural elements of our model, to explain the construction of different laser devices from these elements, to demonstrate the performance of our modeling approach when simulating SRLs, and to perform a spectral analysis of ring lasers, what is very helpful for a better understanding of some numerically observed regimes.

Our paper is organized as follows. In Section 2 we introduce the model equations and the field transmission-reflection conditions at the different interfaces of the complex SRL device. Section 3 gives several examples of different dynamic states. The computation of the optical modes and the explanation of some dynamical regimes are made in Section 4. Finally, some conclusions are drawn in Section 5.

2 Model of the SRL

2.1 Laser configuration

For simulation and analysis of the SRLs we apply our own software `LDSL-tool` [13] used to investigate the (L)ongitudinal (D)ynamics of multisection (S)emiconductor (L)asers. This software allows considering a large variety of laser devices or coupled laser systems composed from different *sections* connected to each other by their edges at some *junctions*: see Fig. 1, where schemes of SRLs considered in Refs. [8, 4, 1, 2, 3, 16] are shown. If needed, we can apply one or several *optical injections* through free edges of some sections: see thick arrows in Fig. 1(b). The *sections*, the *junctions* of these sections and the *optical injections* are three basic structures of our software.

Each *section* S_r can be identified by a unique spatial interval (z'_r, z''_r), where z'_r and z''_r are the spatial coordinates of the section edges, and $z''_r - z'_r$ is the length of S_r. Within each section the spatial-temporal dynamics of the optical fields and the carrier density is governed by the TW model [12]. Passive waveguides and air gaps

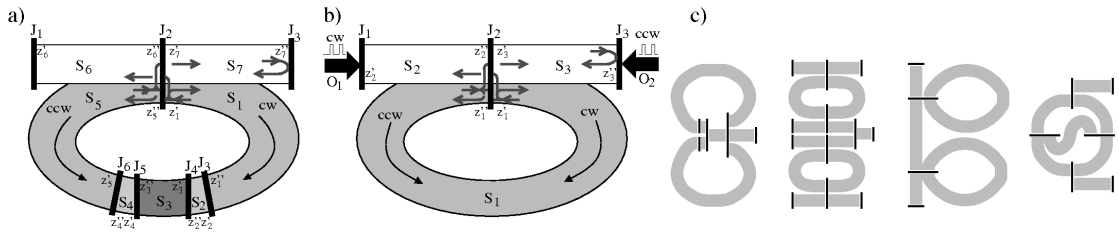

Figure 1: Schemes of several ring laser configurations with indication of sections ($S.$), junctions ($J.$, black intervals), optical injections ($O.$, thick black arrows), propagation directions of the CW and CCW fields (thin black arrows) and some field transmission - reflection - outcoupling directions (grey arrows). (a): an all-active modelocked ring laser with a saturable absorber and (b): a simple ring laser with optical injections as considered in this paper. (c): some other ring laser devices [1, 2, 3, 16] which can be also treated by our software.

between different lasers can also be treated as sections. In this case, one should neglect the carrier rate equations and consider the optical fields alone.

At each *junction* we define the field transmission and reflection conditions. For each edge of all sections we can attribute a unique junction. From the other hand, each junction has at least one section joining it from one or another side: see the black intervals in Fig. 1 indicating all junctions. Some typical junctions of the SRLs considered in this paper are listed below.

First, simple junctions connecting opposite edges of two consequent sections with, possibly, different material or control parameters (e.g., J_3 in Fig. 1a). Second, junctions corresponding to a free edge of some section (e.g., J_1 in Fig. 1a,b). Here we describe a field reflectivity, record an outgoing optical field or apply optical injections. Third, junctions connecting two *left* and two *right* edges and representing a *localized* coupling of the ring laser to the output waveguide (J_2 in Fig. 1a,b).

Finally, each *optical injection* $O(t)$ is attached to a unique junction (e.g., O_1 in Fig. 1(b) is connected to J_1).

2.2 Laser sections

Within each laser section the slowly varying complex counter-propagating optical fields $E(z,t) = (E^+, E^-)^T$, the complex polarization functions $p(z,t) = (p^+, p^-)^T$ and the real carrier density $n(z,t)$ are governed by the TW model. Here, E^+ and E^- denote the CW and CCW propagating fields, respectively. By proper scaling, $|E(z,t)|^2 = |E^+|^2 + |E^-|^2$ is the local photon density.

We consider the Traveling Wave model given in the following form:

$$\begin{aligned}
\partial_t\, E^{\pm}(z,t) &= v_{gr}\left(\left[\mp\partial_z - i\beta^{\pm}\left(n,|E^{\pm}|^2\right)\right]E^{\pm} - \tfrac{\bar{g}}{2}\left(E^{\pm}-p^{\pm}\right) - i\kappa E^{\mp}\right) + F_{sp}^{\pm},\\
\partial_t\, p^{\pm}(z,t) &= \bar{\gamma}(E^{\pm}-p^{\pm}) + i\bar{\omega}p^{\pm},\\
\partial_t\, n(z,t) &= \mathcal{J}(z,t) - R(n) - v_{gr}\Re e\left[\sum_{\nu=\pm} g(n)\sigma_G^{\nu}|E^{\nu}|^2 - \bar{g}E^{\nu *}\left(E^{\nu}-p^{\nu}\right)\right],
\end{aligned} \tag{1}$$

where β^+, β^-, $R(n)$, and $\mathcal{J}(z,t)$ denote the complex propagation factors of the CW and CCW fields, the cubic recombination law, and the non-homogeneous injection model [17]:

$$\begin{aligned}
\beta^{\pm} &= \left(\delta \pm \Delta + \tilde{n}(n)\sigma_I^{\pm}\right) + \tfrac{i}{2}\left(-(\alpha \pm \Delta_{\alpha}) + g(n)\sigma_G^{\pm}\right),\\
\sigma_G^{\pm} &= \left[1+\varepsilon_{Gs}|E^{\pm}|^2 + \varepsilon_{Gc}|E^{\mp}|^2\right]^{-1}, \qquad \sigma_I^{\pm} = \left[1+\varepsilon_{Is}|E^{\pm}|^2 + \varepsilon_{Ic}|E^{\mp}|^2\right]^{-1};\\
R(n) &= \left(\tfrac{n}{\tau_N} + Bn^2 + Cn^3\right), \qquad \mathcal{J}(z,t) = \tfrac{I}{eV} + \tfrac{U_F'}{eVr_s}\left(\tfrac{1}{|S.|}\int_{S.} n(z)dz - n\right).
\end{aligned} \tag{2}$$

The complex factor $\kappa = \kappa_c - i\kappa_d$ is used to describe the *distributed* linear backscattering of the fields, with κ_c and κ_d denoting its conservative and dissipative parts, respectively [4]. Note, that in linear semiconductor lasers this factor is defining the field coupling by Bragg gratings.

The parameters $\bar{g}$, $\bar{\omega}$, and $\bar{\gamma}$ are the amplitude, the central frequency, and the half width at half maximum of the Lorentzian, which fits the material gain profile in the frequency domain [12]. The index change and gain functions $\tilde{n}(n)$ and $g(n)$ can be defined independently of each other. Accordingly, we use different notations for the self- and cross-gain saturation (ε_{Gs}, ε_{Gc}) and for the self- and cross-index saturation (ε_{Is}, ε_{Ic}) coefficients. For simplicity, however, we can assume the commonly used relation $\tilde{n}(n) = \frac{\alpha_H}{2}g(n)$, $g(n) = g'\left(n - n_{tr}\right)$, $\varepsilon_{Gs} = \varepsilon_{Is}$, $\varepsilon_{Gc} = \varepsilon_{Ic}$, with g', α_H and n_{tr} denoting the differential gain, the linewidth enhancement factor, and the transparency carrier density, respectively. In the passive sections, where $\beta^{\pm}$ is independent of n and $|E^{\pm}|^2$, we adjust $g(n) = \tilde{n}(n) = \bar{g} = 0$.

The real parameters v_{gr}, δ, α, Δ and Δ_{α} are the group velocity, the frequency detuning, the mean internal absorption of the fields, the rotation induced frequency detuning between the CW and CCW fields [18], and the asymmetric field absorption [2], respectively. The parameters τ_N, B, C, I, V, U_F', R_s, and e are the linear carrier life time, the bimolecular and Auger recombinations, the current injection, the volume of the active zone in the considered laser section, the derivative of the Fermi level separation, the series resistivity, and the electron charge, respectively. $F_{sp}^{\pm}$ represents the amplified spontaneous emission.

The TW model of similar type was successfully used to simulate dynamics of different multisection semiconductor lasers. In our ring laser case, however, we allow for different propagation factors β^+ and β^-. It will be shown in Section 4 how this difference is responsible for different operation regimes.

2.3 Field transmission and reflection conditions

For completing the TW model (1) we still need to describe the fields *incoming* into the device sections. That is, we need to define the forward (CW) fields E^+ at the left edges z' and the backward (CCW) fields E^- at the right edges z'' of all sections. These values are determined by the fields $E^+(z'',t)$, $E^-(z',t)$ *outgoing* from all sections and by all applied optical injections $O(t)$.

These relations are defined by the following field transmission-reflection conditions at all junctions. Assume that some junction J_s connects the left edges of sections $S_{s'_1},\dots,S_{s'_{\bar{s}'}}$, the right edges of sections $S_{s''_1},\dots,S_{s''_{\bar{s}''}}$, and optical injections $O_{s_1},\dots,O_{s_{\bar{s}}}$. In addition, the factor $s_o = 1$ (or 0) indicates the presence (or the absence) of the field emission from the laser device at this junction. Then the field transmission and reflection conditions at this junction can be defined by the $(\bar{s}'+\bar{s}''+s_o)\times(\bar{s}'+\bar{s}''+\bar{s})$ complex valued matrix $\mathcal{T}_s$:

$$\begin{gathered}\begin{pmatrix}\vec{E}^+_{s'}\\ \vec{E}^-_{s''}\\ E_{\rm out}\end{pmatrix} = \mathcal{T}_s\begin{pmatrix}\vec{E}^+_{s''}\\ \vec{E}^-_{s'}\\ \vec{O}^-_{s}\end{pmatrix}, \qquad \text{where}\\ \vec{E}^{\pm}_{s'} \stackrel{def}{=} \begin{pmatrix}E^{\pm}(z'_{s'_1},t)\\ \vdots\\ E^{\pm}(z'_{s'_{\bar{s}'}},t)\end{pmatrix},\ \vec{E}^{\pm}_{s''} \stackrel{def}{=} \begin{pmatrix}E^{\pm}(z''_{s''_1},t)\\ \vdots\\ E^{\pm}(z''_{s''_{\bar{s}''}},t)\end{pmatrix},\ \vec{O}_{s} \stackrel{def}{=} \begin{pmatrix}O_{s_1}(t)\\ \vdots\\ O_{s_{\bar{s}}}(t)\end{pmatrix},\end{gathered} \tag{3}$$

and $E_{\rm out}$ represents a possible field emission at this junction. To avoid an artificial field amplification, the matrix T_s should satisfy the inequality $\|\mathcal{T}_s\vec{x}\|^2 \le \|\vec{x}\|^2$.

For the typical junctions J_1 and J_2 discussed in Subsection 2.1 and shown in Fig. 1(b) these conditions read as follows:

$$\begin{pmatrix}E^+(z'_2,t)\\ E_{\rm CCW,out}(t)\end{pmatrix} = \begin{pmatrix}-R_1^* & 1\\ T_1 & 0\end{pmatrix}\begin{pmatrix}E^-(z'_2,t)\\ O_1(t)\end{pmatrix}, \qquad |R_1|^2 \le 1,$$

$$\begin{pmatrix}E^+(z'_1,t)\\ E^+(z'_3,t)\\ E^-(z''_1,t)\\ E^-(z''_2,t)\end{pmatrix} = \begin{pmatrix}T_2 & \bar{T}_2 & -R_2^* & 0\\ \bar{T}_2 & T_2 & 0 & 0\\ R_2 & 0 & T_2 & \bar{T}_2\\ 0 & 0 & \bar{T}_2 & T_2\end{pmatrix}\begin{pmatrix}E^+(z''_1,t)\\ E^+(z''_2,t)\\ E^-(z'_1,t)\\ E^-(z'_3,t)\end{pmatrix}, \quad |T_2|^2+|\bar{T}_2|^2+|R_2|^2 \le 1.$$

The real factors T_2 and $\bar{T}_2$ represent the field amplitude *transmission* and *outcoupling* coefficients at J_2, respectively. The non-vanishing field reflection factor R_2 allows us to consider the *localized* linear backscattering of the fields. In general, the estimation of these coefficients requires some more appropriate modeling, which takes into account the curvature of the ring cavity, the field diffraction and the overlapping of the lateral modes in the coupling region [19].

Finally, at all simple *junctions* J_s ($s = 3,4,5,6$ in Fig. 1a) we have $\bar{s}' = \bar{s}'' = 1$, $\bar{s} = s_o = 0$, and $\mathcal{T}_s$ is the 2×2 identity matrix. In some cases, when the heterostructure of these neighboring sections is different, it has sense to introduce non-vanishing off-diagonal terms representing some field reflection at this interface.

3 Examples

The spatial distributions of the optical fields and the carrier density can be important when considering lasers composed from different sections, or when analyzing propagation of optical pulses significantly shorter then the field roundtrip time in the ring cavity.

Modelocked laser. An all-active modelocked ring laser with a saturable absorber [8] (see Fig. 1a) possess both above mentioned properties, which, nevertheless, can be easily treated by our TW modeling approach. One of the observed ML regimes is represented in Fig. 2. The field roundtrip time in the considered laser corresponds to the ∼15 GHz frequency of the ML pulsations. The switching-on of the ML pulsations and their quality (pulse width, jitter, amplitude noise, signal to noise ratio, etc.) can be seen from panels (a-d) of this figure. The field intensity and carrier distributions along the ring cavity at some fixed time moment are shown in Fig. 2(e) and (f), respectively. Here, the abscissa axis represents coordinates on the ring cavity, while the left and right edges of these two diagrams correspond to the position of the localized coupler. The vertical dotted line indicates the symmetric location of the saturable absorber. The nonuniform and non-monotone carrier distribution is a consequence of the counter-propagating short optical pulses which are colliding at the saturable absorber.

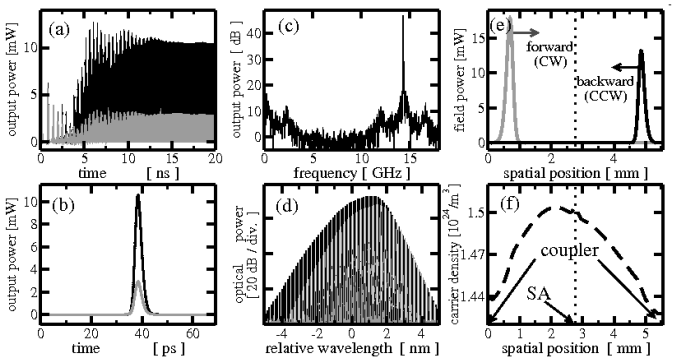

Figure 2: ML regime in the all-active ring laser with the saturable absorber. (a): switching-on of the ML pulsations. (b): sampled pulsating fields. (c,d): radio-frequency (rf) and optical spectra. (e,f): field intensity and carrier distributions along the ring cavity at the fixed time moment. Solid grey and black curves indicate the CW and CCW propagating fields.

Switching between different stable states. In our next example we consider a simple all-active ring laser [5] schematically represented in Fig. 1(b). It is known [4] that these lasers can possess two simultaneously stable stationary states characterized by the dominant contribution of the CW or CCW propagating field (unidirectional bistable regime). We simulate the switching between the stable stationary states by corresponding optical injections

$$O(t) = o(t)Ae^{i\omega t} \qquad \text{with} \qquad \omega = -\frac{2\pi c}{\lambda_0^2}\lambda, \tag{4}$$

where ω, λ, A, $o(t)$, λ_0 and c denote the relative optical frequency and the related wavelength, the amplitude of the injection, the normalized injection profile, the central wavelength, and the speed of light in vacuum, respectively. Grey and black curves in Fig. 3 show the evolution of the outgoing CW and CCW propagating fields. Since we have neglected the linear backscattering, during the unperturbed operation of the laser one of the fields was totally suppressed: see the time traces and the optical spectra of the CW and CCW fields at the initial and the final time intervals, respectively. Within [20, 40]ns time interval we have injected several nearly *resonant* 200 ps long optical pulses traveling in CW and CCW directions: see middle insert of Fig. 3. All these pulses could induce switching between both stable states when applied during the dominance of the opposite field. One can see from Fig. 3 that these switchings can be realized with at least 1GHz repetition frequency.

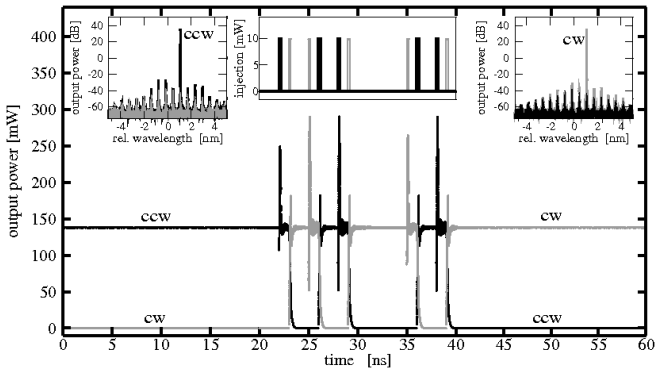

Figure 3: Switching between the CW (grey) and CCW (black) fields by injecting the corresponding optical pulses (middle insert). Optical spectra of the initial and the final states are shown in the left and the right inserts, respectively. The backscattering parameters $\kappa = R_2 = 0$. The bistable operation is induced by the condition $\varepsilon_{Gc} = 2\varepsilon_{Gs}$.

Optical frequency of the injection. In the previous example the switching was imposed by the injection (4) with the optical frequency ω located close to the resonance of the ring cavity. Three such resonances are represented by three peaks of the optical spectra at the top of Fig. 5. Let us consider now the importance of the injection frequency ω for switching between the stationary states. We have performed a series of simulations applying the optical injection (4) with the same injection profile $o(t)$ but different intensity A and relative wavelengths λ. Our observations are summarized in Fig. 4. We have found, that the switching can be realized only for near-resonant injections: compare the optical spectra of the CCW state at the top of Fig. 4 with the injection wavelengths allowing this switching (panels (a,b) of the same figure). We note also the presence of several stable states determined by the ring laser modes at different wavelengths [9]. It is obvious that their presence can not be observed in the simple two mode model [4].

Self- and cross- gain saturation. In the next example we consider the asymmetry of the self- and cross- gain saturations. We have fixed $\varepsilon_{Gs} + \varepsilon_{Gc}$ and have tuned the relative contribution of these factors in the sum: see Fig. 5(a). We have observed four different dynamic regimes, which are represented in panels (b-e) of

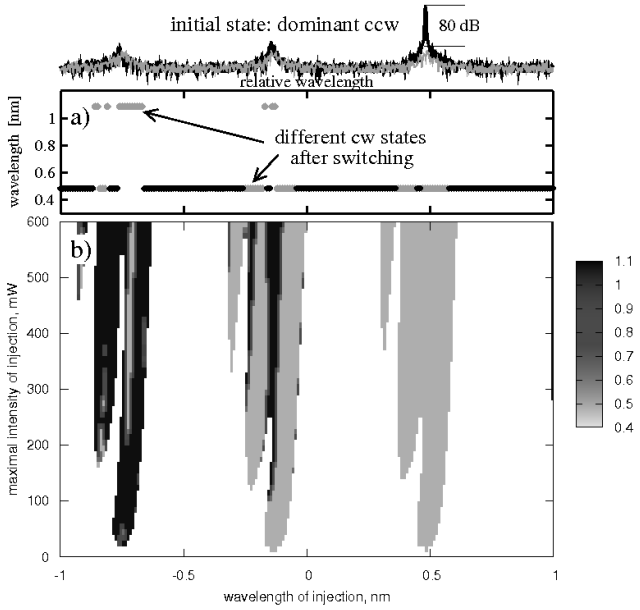

Figure 4: Switching of the initial CCW field (top) by injecting a CW propagating and 100 ps long optical pulse in dependence on the wavelength and the maximal intensity of this pulse. (a): wavelength of the dominant field after the propagation of the injected pulse with 200 mW maximal intensity. Here and at the top: grey and black correspond to the CW and CCW fields. (b): different grey shadings represent the wavelength of the CW field after the successful switching.

the same figure. The first three regimes occurring with a consequent increase of the cross-gain saturation are the bidirectional stable stationary state (b), the alternate oscillations (c), and the unidirectional bistable state (d)[1]. These three regimes are well known already from the two-mode ODE model. The last regime (e) was observed for the dominant cross-gain saturation. Like ML pulsations it is characterized by large short pulses occurring with the ring roundtrip frequency. However, in contrast to the modelocking demonstrated in Fig. 2, this regime is unidirectional and does not require any fast saturable absorption.

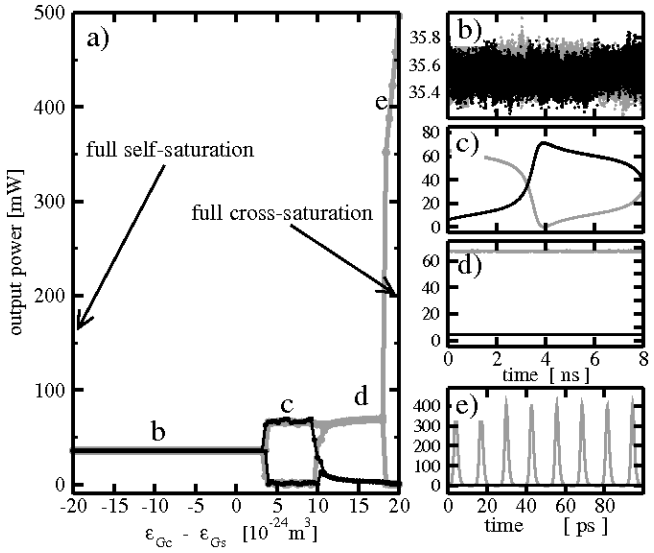

Figure 5: Dynamic regimes for different contributions of the cross- and self- gain saturations. (a): maximal and minimal intensities of the emitted field for different values of $\varepsilon_{Gc} - \varepsilon_{Gs}$. (b-e) typical representatives of the observed regimes. Grey and black: CW and CCW propagating fields. A small distributed coupling ($\kappa|S| = (10 + 0.4i) \cdot 10^{-3}$, $|S|$: length of the ring cavity) was assumed. $\varepsilon_{Gs} + \varepsilon_{Gc} = 20 \cdot 10^{-24}\mathrm{m}^3$.

[1]even though that only one of two available stable stationary states is represented in Fig. 5

4 Mode analysis

The concept of optical modes plays a big role for understanding laser dynamics in general. They represent the natural oscillations of the electromagnetic field and determine the optical frequency and the life time of the photons contained in the given laser cavity. The *instantaneous* optical modes of straight multisection lasers were discussed, e.g., in Ref. [14]. We demonstrate below in this paper how this concept can be applied for analysis of ring lasers.

Let us consider optical modes of the ring cavity alone. That is, we assume that the ring consists of a single or several consequently joined sections $S_1, \dots, S_m$: see, e.g., SRLs shown in Fig. 1(a) with $m = 5$ and (b) with $m = 1$. By $S = [z_1', z_m'']$ and τ we denote the whole ring cavity and the field roundtrip time, respectively. We assume that no external optical fields penetrate the ring cavity, i.e., we have no optical injections nor field reflectivities at the edges of the coupling waveguide.

Within such ring cavity the field and the polarization equations (1) together with the field transmission-reflection conditions (3) can be written in following form:

$$\begin{array}{l} -i\partial_t \Psi(z,t) = H(\beta)\Psi(z,t) + \bar{F}_{sp}, \quad z \in (z_1', z_m''); \\ \left\{ \begin{array}{l} E^+(z_1',t) = TE^+(z_m'',t) - R^* E^-(z_1',t) \\ E^-(z_m'',t) = TE^-(z_1',t) + RE^+(z_m'') \end{array} \right. . \end{array} \tag{5}$$

Here, $\Psi = \binom{E}{p}$ is the field function, and H is a linear $\beta = (\beta^+, \beta^-)$-dependent 4×4 operator.

Optical equations (5) imply the following spectral problem:

$$\Omega(\beta)\Theta(z,\beta) = H(\beta)\Theta(z,\beta), \quad \Theta \stackrel{def}{=} \binom{\Theta_E}{\Theta_p}, \quad \Theta_E \text{ satisfy b.c. from Eq. (5).} \tag{6}$$

The *instantaneous* modes are some $\beta(z,t)$-dependent pairs $(\Omega(\beta), \Theta(z,\beta))$ solving the spectral equation (6). The imaginary and the real parts of the complex eigenvalues Ω are mainly determining the angular frequency and the damping of the corresponding mode [14].

Assume for simplicity[2] a vanishing *distributed* backscattering factor $\kappa = 0$. Then the optical fields within the ring cavity are coupled only indirectly through the propagation factor β. Suppose that for a fixed β we have a complex frequency $\Omega(\beta)$ solving the spectral problem (6). Then we can easily find [14, 15] the field Θ_E and

[2]If $\kappa \neq 0$, many analytic expressions are no more available, and we need to solve the arising problems numerically.

the polarization Θ_p parts of the eigenvector $\Theta(z,\beta)$:

$$\begin{array}{l}
\Theta_E(z,\beta) = \begin{pmatrix} m(\Omega,\bar\beta;z,z''_m)m_\Delta(\Delta_\beta;z,z''_m)s^+ \\ m^{-1}(\Omega,\bar\beta;z,z'_1)m_\Delta(\Delta_\beta;z,z'_1)s^- \end{pmatrix}, \\
\Theta^\pm_p(z,\beta) = \frac{\bar\gamma(z)}{\bar\gamma(z)+i(\Omega-\bar\omega(z))}\Theta^\pm_E(z,\beta), \qquad\qquad \text{where} \\
m(\Omega,\bar\beta;y,x) \stackrel{def}{=} \exp\left(-i\int_x^y\left[\bar\beta(\zeta)+\frac{\Omega}{v_{gr}}+\chi(\Omega,\zeta)\right]d\zeta\right), \\
m_\Delta(\Delta_\beta;y,x) \stackrel{def}{=} e^{-i\int_x^y\Delta_\beta(\zeta)d\zeta}, \qquad \begin{pmatrix} s^+ \\ s^- \end{pmatrix} \stackrel{def}{=} \begin{pmatrix} \Theta^+_E(z''_m,\beta) \\ \Theta^-_E(z'_1,\beta) \end{pmatrix}, \\
\bar\beta \stackrel{def}{=} \frac{\beta^+(z)+\beta^-(z)}{2}, \quad \Delta_\beta \stackrel{def}{=} \frac{\beta^+(z)-\beta^-(z)}{2}, \quad \chi \stackrel{def}{=} -\frac{i\bar g(z)}{2}\frac{i(\Omega-\bar\omega(z))}{\bar\gamma(z)+i(\Omega-\bar\omega(z))}.
\end{array} \tag{7}$$

The complex mode scaling factors $s^\pm$ represent the incoming into the coupler CW and CCW components of Θ_E.

By our assumption Ω and $\Theta^\pm(z,\beta)$ satisfy the spectral problem (6), which can be substituted by the system

$$\begin{cases} m_\Delta(\Delta_\beta;z'_1,z''_m) - m(\Omega,\bar\beta;z''_m,z'_1)T\,s^+ + m(\Omega,\bar\beta;z''_m,z'_1)R^*\,s^- = 0 \\ -m(\Omega,\bar\beta;z''_m,z'_1)R\,s^+ + m_\Delta(\Delta_\beta;z''_m,z'_1) - m(\Omega,\bar\beta;z''_m,z'_1)T\,s^- = 0 \end{cases}, \tag{8}$$

having a nontrivial solution $(s^+,s^-)^T$, i.e., a nonzero eigenfunction $\Theta(z,\beta)$, if only

$$\begin{array}{c}
e^{-i\Omega\tau}e^{-i\langle\chi(\Omega)\rangle} = \mathcal{F}_\pm(\langle\Delta_\beta\rangle,|R|)\,e^{i\langle\bar\beta\rangle}, \qquad \text{where} \qquad \langle y\rangle \stackrel{def}{=} \int_S y(z)dz, \\
\mathcal{F}_\pm(\langle\Delta_\beta\rangle,|R|) \stackrel{def}{=} \frac{T}{T^2+|R|^2}\left[\cos\left(\langle\Delta_\beta\rangle\right) \pm i\left(\sin^2\left(\langle\Delta_\beta\rangle\right)+\frac{|R|^2}{T^2}\right)^{1/2}\right].
\end{array} \tag{9}$$

In the case of a vanishing R we have a simple expression $\mathcal{F}_\pm = \frac{1}{T}\exp\left(\pm i\langle\Delta_\beta\rangle\right)$.

A set of all complex numbers Ω solving Eq. (9) coincide with the set of all eigenvalues of the spectral problem (6). Assuming that the gain dispersion function $\chi(\Omega)$ is small we can get the approximations

$$\Omega_{k^\nu} \approx \frac{\left[2\pi k - \langle\bar\beta\rangle - \arg\left(\mathcal{F}_\nu(\langle\Delta_\beta\rangle,|R|)\right) + i\log\left|\mathcal{F}_\nu(\langle\Delta_\beta\rangle,|R|)\right|\right]}{\tau}, \ \nu=\pm, \ k\in\mathbf{Z}, \tag{10}$$

of the most important eigenvalues[3] which we can later improve numerically [14]: see Fig. 6.

Formula (10) shows that the eigenvalues Ω_{k^ν} are appearing in pairs ($\nu=\pm$), and the different pairs are separated by the roundtrip frequency $\frac{2\pi}{\tau}$. A less obvious separation of the eigenvalues Ω_{k^+} and Ω_{k^-} can be understood by considering the expression of $\mathcal{F}_\pm$ given in Eq. (9). The nontrivial factor $\Im m\langle\Delta_\beta\rangle$ (induced by non-vanishing Δ_α or $\varepsilon_{Gs}-\varepsilon_{Gc}$) is mainly responsible for the separation of the imaginary parts (gain thresholds) of $\Omega_{k^\pm}$. Similarly, the separation of the real parts (frequencies) of $\Omega_{k^\pm}$ is mainly due to non-vanishing R or $\Re e\langle\Delta_\beta\rangle$ (i.e., non-vanishing Δ and $\varepsilon_{Is}-\varepsilon_{Ic}$).

[3]Other roots of Eq. (9) are due to the non-vanishing nonlinear function $\chi(\Omega,z)$. However, all these roots have large positive imaginary parts [20], and the corresponding modes are well damped.

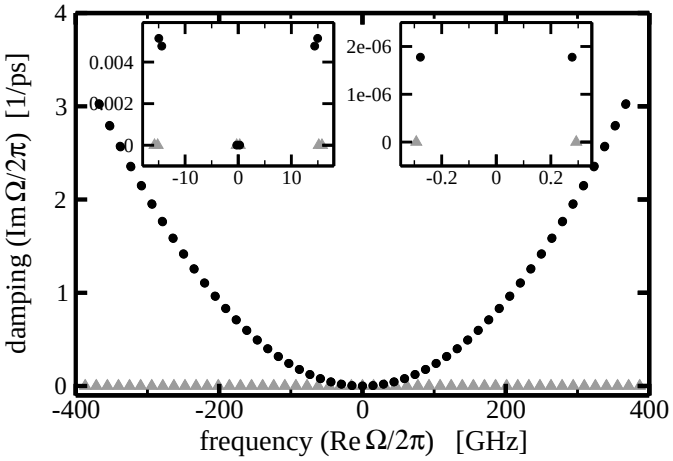

Figure 6: Main roots Ω of Eq. (9) (black bullets) and their initial approximations given by Eq. (10) (grey triangles) for some fixed $\beta(z)$ with $\langle\bar{\beta}\rangle = 0$. Inserts: the vicinity of the zero frequency showing closely located pairs $(\Omega_{k^+}, \Omega_{k^-})$. Parameters κ, Δ, Δ_α, ε_{Is}, ε_{Ic}, $\bar{\omega}$ are set to zero. $\varepsilon_{Gs} = \varepsilon_{Gc} \neq 0$, $R = 0.1$, $T = \sqrt{0.7}$.

Mode beating. Fig. 6 gives an illustration of this statement. The mode splitting here is imposed by $R \neq 0$, while $\langle\Delta_\beta\rangle = 0$. Since the thresholds of the modes k^+ and k^- are similar one can expect both of them contributing to the dynamics of the optical fields producing beating type pulsations with the beat frequency $f_{slow} \approx |\Re e\,(\Omega_{k^+} - \Omega_{k^-})|\,/2\pi$. And indeed, this type of dynamics was observed: see Fig. 7. Panels (a) and (b) of this figure indicate the presence of two characteristic frequencies of this regime. The slow frequency f_{slow} coincides perfectly with the mode pair frequency separation formula given a few lines above. This agreement is also illustrated in Fig. 7(c,d): compare the mode separation in (c) and the separation of the spectral peaks in (d). The less pronounced fast frequency f_{fast} in Fig. 7(b) corresponds to the field roundtrip time in the ring cavity, i.e., to the frequency separation of the neighboring mode pairs: $|\Omega_{k^\pm} - \Omega_{(k-1)^\pm}|/2\pi$.

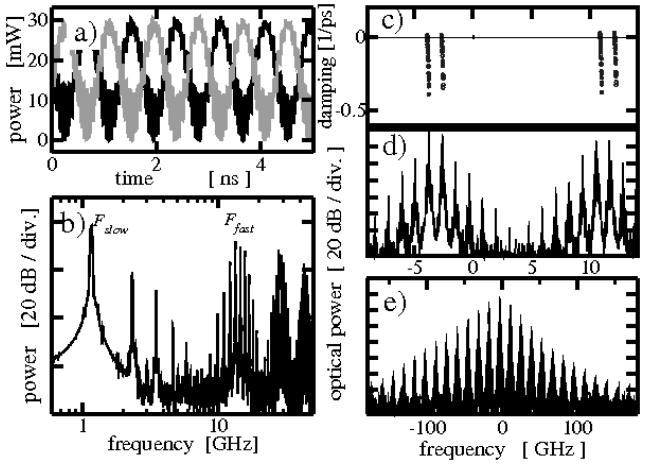

Figure 7: A dynamic regime induced by beating of different modes. (a): intensity of the outgoing CCW (grey) and CW (black) field. (b): rf spectra of the outgoing CW field (note the logarithmic scale of the frequency axis). (c): four main eigenvalues $\Omega(\beta(t))$ at several time instants t. (d,e): optical spectra. Parameters as in Fig. 6.

Stability of unidirectional states. The mode spectra can also explain the stability or the instability of stationary (rotational wave) states determined by some modes with *real* eigenvalues Ω:

$$(\Psi(z,t), n(t)) = \left(\Theta(z,\beta)e^{i\omega t}, \bar{n}\right), \quad \text{where} \quad \Omega(\beta) = \omega \in \mathbf{R}.$$

To make the explanation more transparent, let us consider a simple case with $R = \chi(\omega) = \Delta_\alpha = 0$.

Let us assume the complex factor $s^+ \neq 0$ (we have a non-vanishing emission of the CW field). As it follows from Eqs. (8,10), the angular frequency ω of this state can be identified with some eigenvalue Ω_{k^+}. In the same manner, the assumption $s^- \neq 0$ (a non-vanishing emission of the CCW field) implies $\omega = \Omega_{k^-}$. Thus, both non-vanishing fields are available if only $\Omega k^+ = \Omega_{k^-}$ what can be realized only for $\langle\Delta_\beta\rangle = 0 \bmod(\pi)$.

In the unidirectional stationary state determined by, for example, k^+-th mode we have $s^+ \neq 0$, $s^- = 0$, $\Omega_{k^+} = \omega$ and $\Omega_{k^-} = \omega + \frac{2\langle\Delta_\beta\rangle}{\tau}$. The dominance of the cross-gain saturation over the self-saturation ($\varepsilon_{Gc} > \varepsilon_{Gs}$) and notations (2) imply the inequalities $\Im m\langle\Delta_\beta\rangle > 0$, $\Im m\Omega_{k^-} > 0$, what indicate damping of this neighboring k^--th mode. Thus, one can expect a stable operation at this unidirectional stationary state: see Fig. 5(d), where we could demonstrate such regime even in the presence of some small backscattering factor κ. In the opposite ($\varepsilon_{Gc} < \varepsilon_{Gs}$) case we have $\Im m\langle\Delta_\beta\rangle > 0 > \Im m\Omega_{k^-}$, what implies the growth of k^--th mode and, therefore, the instability of this unidirectional stationary state.

We admit, however, that this *mode* analysis gives only hints, whether some state can be stable or not. The performance of the accurate stability analysis is much more demanding problem and is out of the scope of the present paper.

5 Conclusions

The traveling wave model can be used for simulating and analyzing the nonlinear dynamics in various semiconductor ring laser devices. This model could recover Typical operation regimes such as bistable unidirectional and stable bidirectional stationary states, or alternate oscillations known from experiments and modeling with a simple two-mode ODE model can also be recovered by the TW model. Moreover, our model can also reproduce typical multi-mode regimes such as multiple stable states, mode jumping or modelocking pulsations, which are not accessible to the simple ODE model. In addition, we have shown how computation of optical modes may help us for understanding the observed dynamical regimes.

Acknowledgments

This work was supported by DFG Research Center MATHEON "Mathematics for key technologies: Modelling, simulation, and optimization of real-world processes".

References

[1] S. Zhang, Y. Liu, D. Lenstra, M.T. Hill, H. Yu, G.D. Khoe, H.J.S. Dorren: "Ring-laser optical flip-flop memory with single active element", *IEEE J. Sel. Topics Quantum Electron.*, **10**, p. 1093, 2004.

[2] H. Cao, C. Liu, H. Ling, H. Deng, M. Benavidez, V.A. Smagley, R.B. Caldwell, G.M. Peake, G.A. Smolyakov, P.G. Eliseev, M. Osinski: "Frequency beating between monolithically integrated semiconductor ring lasers", *Appl. Phys. Lett.*, **86**, art.no. 041101, 2005.

[3] M.T. Hill, H.J.S. Dorren, T. de Vries, X.J.M. Leijtens, J.H. den Besten, B. Smalbrugge, Y.-S. Oei, H. Binsma, G.-D. Khoe, M.K. Smit: "A fast low-power optical memory based on coupled micro-ring lasers", *Nature*, **432**, pp. 206–209, 2004.

[4] M. Sorel, G. Giuliani, A. Scire, R. Miglierina, J.P.R. Laybourn, S. Donati: "Operating regimes of GaAs-AlGaAs semiconductor ring lasers: experiment and model", *IEEE J. Quantum Electron.*, **39**(10), pp. 1187–1195, 2003.

[5] A. Perez, A. Scire: "Bistability and all-optical switching in semiconductor ring lasers", *Optics Express*, **15**(20), pp. 12941–12948, 2007.

[6] E.J. Doedel, A.R. Champneys, T.F. Fairgrieve, Yu.A. Kuznetsov, B. Sandstede, and X. Wang, "AUTO97: Continuation and bifurcation software for ordinary differential equations (with HomCont)", *Technical report*, Concordia University, 1997.

[7] G. Van der Sande, L. Gelens, P. Tassin, A. Scire, J. Danckaert: "Two-dimensional phase-space analysis and bifurcation study of the dynamical behaviour of a semiconductor ring laser", *to appear in J. of Phys. B*, **41**, April 2008.

[8] Y. Barbarin, E.A.J.M. Bente, M.R.J. Heck, Y.S. Oei, R. Nötzel, M.K. Smit: "Characterization of a 15 GHz integrated bulk InGaAsP passively modelocked ring laser at 1.53 μm", *Optics Express*, **14**(21), pp. 9716–9727, 2006.

[9] C. Born, S. Yu, M. Sorel, P.J.R. Laybourn: "Controllable and stable mode selection in a semiconductor ring laser by injection locking", *Proc. CLEO*, pp. 1275–1276, 2003.

[10] I. Stamataki, S. Mikroulis, A. Kapsalis, D. Syvridis: "Investigation on the multimode dynamics of InGaAsP-InP microring lasers", *IEEE J. Quantum Electron.*, **42**(12), pp. 1266–1273, 2006.

[11] A.G. Vladimirov, D. Turaev: "Model for passive mode-locking in semiconductor lasers", *Phys. Rev. A*, **72**(3), art. no. 033808, 2005.

[12] U. Bandelow, M. Radziunas, J. Sieber, and M. Wolfrum: "Impact of gain dispersion on the spatio-temporal dynamics of multisection lasers", *IEEE J. Quantum Electron.*, **37**, pp. 183–188, 2001.

[13] `http://www.wias-berlin.de/software/ldsl`

[14] M. Radziunas, H.-J. Wünsche, "Multisection Lasers: Longitudinal Modes and their Dynamics", Chapter 5 in *Optoelectronic Devices: advanced simulation and analysis*, ed. J. Piprek, Springer, pp. 121–150, 2005.

[15] M. Radziunas, "Numerical bifurcation analysis of the traveling wave model of multisection semiconductor lasers", *Physica D*, **213**, pp. 98–112, 2006.

[16] J.P. Hohimer, G.A. Vawter, D.C. Craft: "Unidirectional operation in a semiconductor ring diode laser", *Appl. Phys. Lett.*, **62**(11), pp. 1185–1187, 1993.

[17] U. Bandelow, H. Wenzel, H.-J. Wünsche: "Influence of inhomogeneous injection on sidemode suppression in strongly coupled DFB semiconductor lasers", *Electron. Lett.*, **28**, pp. 1324–1326, 1992.

[18] A. Perez, A. Scire: "Theoretical analysis of a new technique for inertial rotation sensing using a semiconductor ring laser", *submitted to IEEE Photon. Techn. Lett.*, 2008.

[19] T. Krauss, P.J.R. Laybourn: "Very low threshold current operation of semiconductor ring lasers", *IEE Proc.-J*, **139**(6), pp. 383–388, 1992.

[20] J. Sieber: "Longitudinal dynamics of semiconductor lasers", PhD Thesis, faculty of Mathematics and Natural Sciences II, Humboldt-University of Berlin, 2001.